MID-AMERICA TRANSPORTATION CENTER

Report # MATC-UI: 141-1

Final Report
WBS:25-1121-0005-141-1

Development of New Design Guidelines for Protection against Erosion at Bridge Abutments Phase II

George Constantinescu, Ph.D.
Professor
Department of Civil and Environmental Engineering
The University of Iowa

Hao Wu
Graduate Research Assistant

2020

A Cooperative Research Project sponsored by
U.S. Department of Transportation- Office of the Assistant Secretary for Research and Technology

Development of New Design Guidelines for Protection against Erosion at Bridge Abutments Phase II

George Constantinescu, Ph.D., PI
Professor
Department of Civil and Environmental Engineering
The University of Iowa

Hao Wu
Graduate Research Assistant
Department of Civil and Environmental Engineering
The University of Iowa

A Report on Research Sponsored by

Mid-America Transportation Center

University of Nebraska–Lincoln

January 2020

Technical Report Documentation Page

1. Report No. 25-1121-0005-141-2	2. Government Accession No.	3. Recipient's Catalog No.
4. Title and Subtitle Development of New Design Guidelines for Protection against Erosion at Bridge Abutments		5. Report Date January 2020 6. Performing Organization Code
7. Author(s) George Constantinescu, Ph.D., PI ORCID: https://orcid.org/0000-0001-7060-8378 Hao Wu		8. Performing Organization Report No. 25-1121-0005-141-2
9. Performing Organization Name and Address Department of Civil and Environmental Engineering The University of Iowa Iowa City, IA 52242		10. Work Unit No. 11. Contract or Grant No. 69A3551747107
12. Sponsoring Agency Name and Address Mid-America Transportation Center 2200 Vine St. PO Box 830851 Lincoln, NE 68583-0851		13. Type of Report and Period Covered Final Report May 2017-May 2018 14. Sponsoring Agency Code MATC TRB RiP No. 91994-25
15. Supplementary Notes Conducted in cooperation with the U.S. Department of Transportation, Federal Highway Administration.		

16. Abstract

Severe floods in the United States Midwest have caused major erosion at bridge abutments despite the fact that their protection design measures followed existing guidelines (e.g., HEC 23, 2001 and following updates through 2009). One likely possibility for the severe bridge erosion observed especially at small bridges is that the methodology to estimate the variables in the design formulas (e.g., for the minimum size of the riprap stone used for protection) recommended in these guidelines is oversimplified and/or does not account for complexities associated with these structured being placed in natural streams where, for instance, bank curvature effects may be important. The present research proposes a numerically-based approach for improving methodologies to design riprap protection measures at wing-wall and spill-through abutments. The mean flow fields and the bed shear stress distributions are obtained from fully three-dimensional, non-hydrostatic RANS simulations. These data are used to estimate the maximum bed shear stress over the riprap layer, the shear-failure entrainment threshold for the riprap stone and the other variables in the design formulas recommended in HEC 23 (Lagasse et al., 2001, Pagan-Ortiz, 1991). The numerically-based approach was validated for the case of wing-wall abutments placed in a straight channel based on data from laboratory experiments. The present Year 2 report describes how channel curvature and floodplain width affect the maximum bed shear stress over the region protected by riprap for wing-wall abutments placed at the two sides of a channel containing a floodplain at its two sides. A modified, two parameter, design formula is proposed that explicitly incorporates the effects of bank curvature and floodplain width.

17. Key Words Bridges, Bridge scour, Bridge abutment, Local Scour, Rip-rap protection against scour	18. Distribution Statement No restrictions. This document is available through the National Technical Information Service, Springfield, VA 22161.		
19. Security Classif. (of this report) Unclassified	20. Security Classif. (of this page) Unclassified	21. No. of Pages xx	22. Price

Form DOT F 1700.7 (8-72) Reproduction of completed page authorized

Table of Contents

List of Figures

List of Tables

Acknowledgments

We would like to thank Prof. Bruce Melville form University of Auckland, New Zeeland for providing additional information on his experiments carried for wing-wall abutments.

Disclaimer

The contents of this report reflect the views of the authors, who are responsible for the facts and the accuracy of the information presented herein. This document is disseminated in the interest of information exchange. The report is funded, partially or entirely, by a grant from the U.S. Department of Transportation's University Transportation Centers Program. However, the U.S. Government assumes no liability for the contents or use thereof.

Abstract

Severe floods in the United States Midwest have caused major erosion at bridge abutments despite the fact that their protection design measures followed existing guidelines (e.g., HEC 23, 2001 and following updates through 2009). Placing riprap stone around the base of the abutment (e.g., in the form of an apron) and over its erodible faces is the most common way to protect abutments against erosion (e.g., see NCHRP Projects 24-18, 24-19, 24-20). One likely possibility for the severe bridge erosion observed especially at small bridges is that existing design formulas to calculate the minimum size of the riprap stone used for protection of wing-wall and spill-through abutments (e.g., Lagasse et al., 2001; Pagan-Ortiz, 1991) are based on an oversimplified approach. Moreover, such formulas do not account for complexities associated with these structures being placed in natural streams where, for instance, bank curvature effects may be important. The coefficients in these formulas were determined based on a limited series of laboratory experiments conducted for a relatively narrow range of relevant geometrical and flow parameters that influence the flow erosion capability at such bridge sites.

This project aims to improve the performance and range of applicability of riprap design formulas used for erosion protection at wing-wall and spill-through abutments. These two types of abutments are often installed over the floodplain for small bridges without piers. Spill-through abutments are also used for large bridges.

The mean flow fields and the bed shear stress distributions are obtained from fully three-dimensional, non-hydrostatic RANS simulations. These data are then used to estimate the maximum bed shear stress over the riprap apron, the shear-failure entrainment threshold for the riprap stone and the other variables in the design formulas recommended in HEC 23 (Lagasse et al., 2001, Pagan-Ortiz, 1991). The numerically-based approach was validated for the case of

wing-wall abutments placed in a straight channel based on data from laboratory experiments. The present Year 2 report describes how channel curvature and floodplain width affect the maximum bed shear stress over the region protected by riprap for wing-wall abutments placed over the floodplains of a channel. Using data obtained from numerical experiments, the Year 2 report focuses on incorporating the effects of bank curvature and floodplain width in a new riprap size design formula for protection of wing-wall abutments against erosion.

Chapter 1 Introduction

1.1 Motivation

Severe erosion problems were reported at many bridge sites in the US, especially for abutments and embankments of smaller-size bridges. This is especially a problem of great concern in the Midwest where a large number of small bridges are present in rural areas. In extreme cases, e.g. during large floods when overtopping occurs, the embankments of such small bridges can be washed away (Figure 1.1). Two of the most encountered types of abutments used at such bridges are spill-through and wing-wall abutments. The most common type of erosion protection measure is to place riprap stone around the base of the abutment in the region where scour is expected to develop. This layer of riprap stone is commonly referred as an apron. The increased size/weight of the riprap stones enables them to resist the increased velocities and turbulence caused by the presence of the abutment in the flow. Thus the riprap apron provides an armor layer protection to the underlying finer sediments. The riprap stone forming the abutment apron may be subjected to several modes of failure including shear failure, winnowing failure, and edge failure (Melville et al., 2007). In general, the minimum size of the riprap stone in design equations is determined such that shear and edge failure are avoided (Melville et al., 2007). Shear failure occurs where the individual riprap stones are not large enough to resist entrainment by the flow.

Figure 1.1 Effect of flood on erosion at a small bridge situated in Squaw Creek, close to Ames (Iowa). The left picture shows that all the erodible material behind the toe of the wing-wall abutment was washed by the flood. The right picture shows the bridge after the abutments were reconstructed and riprap stone was placed on the floodplain around the abutments

Severe erosion problems were even reported at some bridge abutments where riprap protection measures followed existing design guidelines (e.g., as outlined in the Hydraulic Engineering Circular HEC-23, 2001 and following updates - 2009). In general, design guidelines for bridge piers and abutments (e.g., Hoffmans and Verheij, 1997, Lagasse et al., 2001, Sumer and Fredsoe, 2002, Melville and Coleman, 2000, Melville et al., 2006a, 2006b, Cardoso et al., 2010, Ettema et al., 2011) are mostly based on laboratory experiments (flume studies) conducted for a limited range of flow conditions (e.g., straight channels, limited width of the floodplain). None of these design formulas can be used for cases when bank curvature effects are important or pressure scour effects due to bridge deck submergence are present. Thus, there is a need to improve these guidelines and propose modified formulas or methodologies that can provide effective protection against erosion for a larger range of flow and geometrical conditions at these two types of abutments.

1.2 Prior Main Results and Findings

During Year 1, 3-D RANS simulations were performed for wing-wall and spill-through abutments placed in a straight channel. Figure 1.2 shows the general layout of the computational domain and the main geometrical variables (B_f=floodplain width, L_a=abutment length, y_m=flow depth over main channel, y_f=flow depth over floodplain), as well as the position of the riprap apron. Outside of the riprap apron, the flat bed was covered with sand with d_{50}=0.82 mm. The inlet discharge was varied until the maximum value of the bed friction velocity over the riprap layer was $0.35u_{*cr}$, where u_{*cr} is obtained from the Shields diagram for a given mean diameter of the riprap stone, D_{50}. Following Melville and Coleman (2000), this value was used to determine the riprap shear failure entrainment threshold. The Froude number, Fr, was calculated using the mean velocity in the section containing the abutment.

For wing-wall abutments, simulations were conducted with flow only inside the main channel (y_m=0.1 m) and with flow over the floodplain (y_m=0.17 m, y_f=0.07 m) for B_f=0.4 m and 1.4 m and 20 mm<D_{50}<61 mm. Five of the simulated test cases of the wing-wall abutment corresponded to those in the experiments of Melville et al. (2007). Figure 1.3 shows that for each of the five series of experiments, the numerically predicted shear failure entrainment threshold was situated in between the limiting experiments where no shear failure and, respectively, shear failure were observed. This result is of great importance as it validates the proposed numerical approach to determine the entrainment threshold for the riprap stone. Also represented are the design formulas of Pagan-Ortiz (1991) $D_{50}/y=(1.064/(S_s-1))^{0.81}$ *$Fr^{1.62}$ and Lagasse et al. (2001) $D_{50}/y=(K_s/(S_s-1))$*Fr^{α} where the shape factor is K_s=1.02 and the power law exponent is α=2 for Fr<0.8, K_s=0.69 and α=0.28 for Fr>0.8, S_s=2.65 is the specific gravity of the riprap stone and $y=y_m$ for wing-wall abutments.

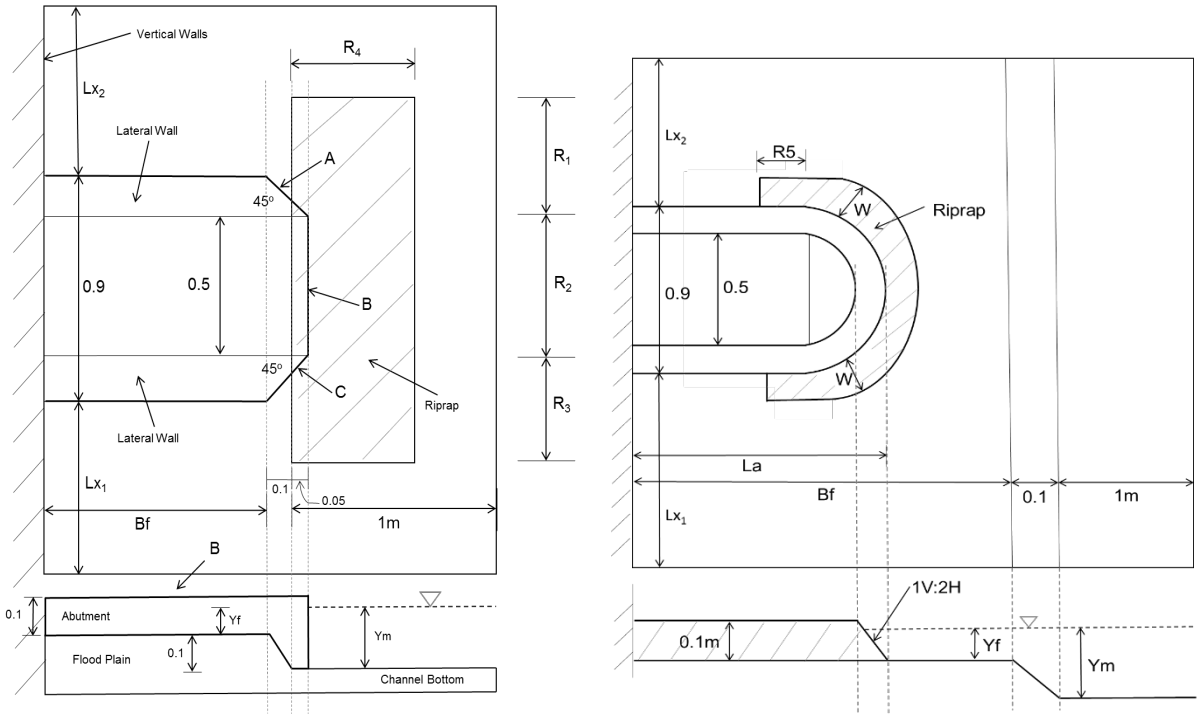

Figure 1.2 Sketch showing general layout of the preliminary numerical simulations performed for a wing-wall abutment (left) and for a spill-through abutment (right) placed on the floodplain of a straight channel. Dimensions are in meters. The wing-wall abutment geometrical set up corresponds to that used in the laboratory experiments of Melville et al. (2007). Reproduced from Wu et al. (2019).

Based on a limited number of simulations conducted for wing-wall abutments placed in a straight channel, it was also concluded that the original Lagasse et al. (2001) formula is conservative enough only for high-flow cases with relatively narrow floodplains (e.g., B_f=0.4 m). One main recommendation was to modify this formula and use K_s=1.65 or, even better, to specify K_s as a function of the relative width of the floodplain (B_f/y_m). That study also found the Pagan-Ortiz (1991) formula gives excellent predictions of the entrainment threshold for cases where the floodplain was not flooded.

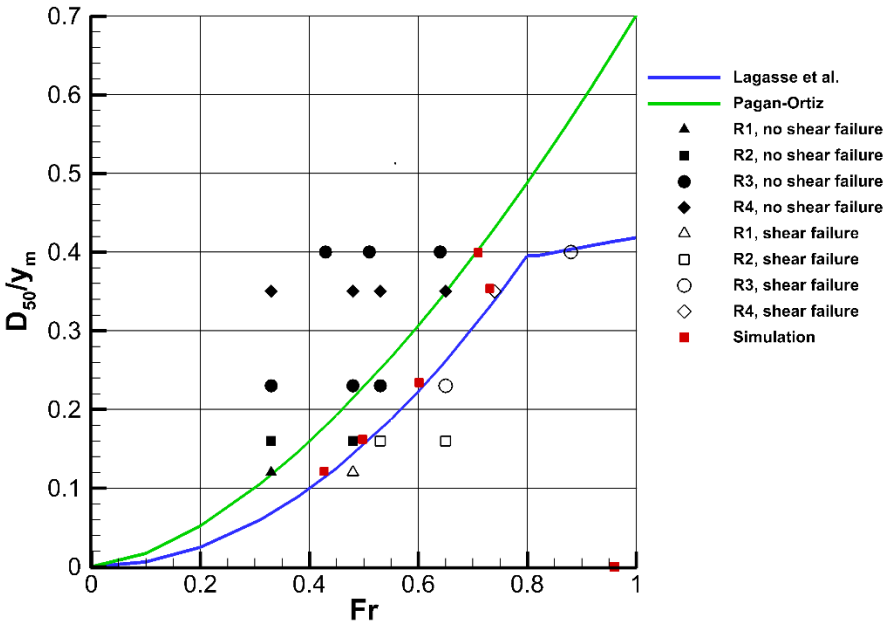

Figure 1.3 Comparison of numerical results with Lagasse et al. (2001) and Pagan-Ortiz (1991) equations and the experimental data of Melville et al. (2007) for a wing-wall abutment in a straight channel. Simulation data always show predicted conditions for treshold of riprap stone entrainment by shear failure. Experimental data only show if shear failure occurred (open symbols or not (solid symbols) in the corresponding experiments. Reproduced from Wu et al. (2019).

1.3 Objectives

As discussed in section 1.1, there is a clear need to conduct new research to better address the fundamental aspects of the scour protection design guidelines for abutments in HEC 23. The proposed numerical approach to estimate maximum bed shear stress and to evaluate the critical Froude number at which entrainment of riprap stone of a certain diameter occurs was validated during Year 1. The main research objectives for Year 2 are to:

1. Perform a comprehensive set of numerical experiments to determine the shear-failure entrainment threshold for the riprap apron protecting wing-wall abutments positioned on the floodplain of a curved channel over a relevant range of the (nondimensional) radius of curvature of the channel,

2. Test performance of main design formulas recommended by HEC 23 (Lagasse et al., 2001; Pagan-Ortiz, 1991) to estimate minimum size of the riprap stone used for protection against erosion for wing-wall abutments placed in straight and curved channels with/without a floodplain, and
3. Propose a design formula that can be applied for wing-wall abutments placed in both straight and curved channels and that incorporates the effect of the nondimensional floodplain width.

1.4 Justification of Research Approach

Understanding and being able to quantitatively describe how the hydrodynamics of the stream flow field (velocity magnitude and bed shear stress distributions around the bridge site) changes with increasing stage and discharge as a result of a flood is critical to be able to propose effective measures to protect bridge abutments and piers against erosion. The National cooperative Highway Research Program Report 587 (NCHRP Report 587) used in the development of HEC 23 (2001, 2009) states the following:

> Selection of countermeasures to protect bridges from scour requires estimates of velocity distributions in the bridge opening. Estimates of the peak velocity in what is typically a highly non-uniform flow distribution near the tip of the abutment is necessary to determine whether countermeasures are necessary and, if so, to determine the type, size, and extent of countermeasures to protect bridge abutments from scour. Laboratory physical models have been developed to determine the size, type, and location of protection for a relatively small range of flow conditions at bridges; however, the laboratory models represent very simplistic geometric conditions. Effective transfer of laboratory model results to the complex hydrodynamic conditions of real bridge sites requires that flow velocity be predicted in the vicinity of bridge abutments using numerical models.

The report also comments on the limitations of the two-dimensional (2-D) depth-averaged modeling approach which was used in past studies to provide more accurate estimations of the variables in the design formulas used to protect against erosion. The main

limitations of the 2-D approach are due to the hydrostatic pressure assumption and simplified turbulence modeling. Moreover, the region of maximum velocity amplification near the abutment toe is generally located in a region of high flow curvature and, in many cases, it is situated over a sloped surface where such 2-D numerical simulations give relatively large errors.

The present study uses fully three-dimensional (3-D), non-hydrostatic, RANS simulations performed on fine meshes to obtain the 3-D velocity flow field. This allows direct estimation of the boundary shear stress over the whole bed region, including over the riprap apron. For each set of geometrical and flow conditions, the 3-D RANS simulation results are then used to estimate the maximum shear stress over the riprap region. This bed shear stress is then compared with the critical value for riprap failure given a certain mean size of the riprap stone. The approach of Melville and Coleman (2000) and Melville et al. (2007) is used to determine if riprap stone shear failure will occur or not. In particular, this methodology can be used to test the performance of the leading design formulas recommended by HEC 23 for erosion protection of bridge abutments using riprap stone.

Given the detailed information on the flow fields, turbulence and their effects on the bed shear stress distributions available from such 3-D simulations, the proposed approach can lead to extension of the range of geometrical and flow configurations for which design formulas can be applied (e.g., abutments placed inside or immediately downstream of curved channels, high flow conditions that lead to the bridge deck becoming submerged). For such cases, laboratory experiments are very expensive and the range of geometrical (e.g., channel aspect ratio, width of the floodplain) and flow parameters in these experiments are even more limited compared to the simpler case of an abutment placed in a straight channel. The numerically-based approach adopted in the present study does not face these limitations. Moreover, this approach can also be

applied for cases when pressure scour effects are significant, something that is impossible to be achieved using 1-D and 2-D numerical models.

Chapter 2 Numerical Method

STAR-CCM+ is a state-of-the-art commercial code developed by CD-Adapco which solves the fully 3-D non-hydrostatic Navier-Stokes equations using the finite volume method on structured/unstructured meshes. The RANS turbulence model provides the value of the eddy viscosity. The governing continuity and momentum equations are:

$$\frac{\partial U_i}{\partial x_i} = 0 \tag{2.1}$$

$$\frac{\partial U_i}{\partial t} + \frac{\partial (U_i U_k)}{\partial x_k} = -\frac{1}{\rho}\frac{\partial P}{\partial x_i} + \frac{1}{\rho}\frac{\partial}{\partial x_k}\left[(\mu + \mu_t)\left(\frac{\partial U_i}{\partial x_k} + \frac{\partial U_k}{\partial x_i}\right)\right] - g\hat{k} \tag{2.2}$$

where

U_i = Reynolds Averaged velocity component along the i direction

ρ = fluid density

μ = molecular dynamic viscosity

μ_t = eddy viscosity calculated from the RANS turbulence model

P = pressure

g = gravitational acceleration

$\hat{k}$ = unit normal vector along the vertical direction

The discretised RANS equations are solved using a fractional-step algorithm. The advective terms are discretised using the second-order accurate upwind scheme, while the transient term discretization in time is second-order accurate based on an implicit representation. The diffusive terms and the pressure gradient terms are discretised using the second-order

accurate central scheme. The pressure-coupling is achieved using the SIMPLE algorithm. In the SIMPLE algorithm, the momentum equations without the pressure gradient term are advanced in time and an intermediate velocity is obtained which does not satisfy the continuity equation. A pressure-correction algorithm is then employed to modify the pressure field such that mass conservation is achieved.

Several two-equation turbulence models available in STARCCM+ were initially considered. The k-w SST model performed more accurately for channel flow simulations with a large value of the relative bed roughness, leading to its use in the simulations reported in this paper. STAR CCM+ with the k-w SST turbulence model was widely used and validated for predictions of flow in channels containing hydraulic structures (Cheng et al., 2018), including for cases when an unsteady flood wave advanced in a channel with natural bathymetry (Cheng et al., 2018 and Horna-Munoz and Constantinescu, 2016, 2018).

No-slip boundary conditions were specified at all wall boundaries. The bed shear was calculated using the law of the wall. At the rough-wall boundaries, the specified value of the surface roughness k_s was different over the riprap region and over the rest of the channel bed that was assumed to be covered by a layer of sand. The outlet was specified as a pressure outlet boundary. The free surface was treated as a slip (symmetry) boundary on which the vertical velocity was set equal to zero. Preliminary straight and curved channel flow, steady RANS simulations with periodic boundary conditions in the streamwise direction were performed to obtain a fully developed channel flow solution to be used to specify the inlet boundary condition in the corresponding simulations of flow in channels containing abutments. The cross section of the channel used in the preliminary simulations was identical to the inlet section of the computational domain in the simulations where abutments were present. The 2-D distributions of

the velocity and the turbulence variables from the periodic simulations were specified at the inlet of the domain containing the abutments. All simulations were performed in domains containing abutments at both sides of the channel. This is needed because in the case of curved channels the flow field is not symmetrical with respect to the axis of the main channel. Given that domains with abutments at both sides have to be considered for the curved channel simulations, we decided to redo all Year 1 simulations for wing-wall abutments placed in a channel of half channel width in a computational domain containing both abutments. The number of cells in the new simulations was about two times larger than that in the simulations discussed in the Year 1 Report.

STAR-CCM+ contains a very powerful meshing capability in which an initial geometry can be imported and smoothed in such a way to improve computational efficiency without loss of critical information. Once the geometry has been processed, a volume mesh is created with the desired meshing model to obtain a high-quality mesh. The grid generator allows the use of various controls and the generation of fine meshes in different parts of the domain where flow resolution needs to be higher (e.g., near the solid surfaces to resolve the attached boundary layers), which is essential to generate a high quality mesh. One of the main advantages of the grid generator in STARCCM+ is that it allows automatic grid refinement in critical regions situated around the abutments with a smooth transition to regions where the mesh is coarser.

Chapter 3 Wing-Wall Abutments Placed in Straight and Curved Channels

In some cases, bridges are built inside, or immediately downstream, of regions where bank curvature is important. In such cases, the approaching velocity field around the abutment is quite different compared to the case of a straight channel, with a large streamwise velocity amplification occurring close to the abutment situated at the outer bank of the curved channel, at least for moderate channel curvatures. High-flow conditions where the floodplain becomes submerged add to the flow complexity for cases when abutments are situated inside or close to regions where the channel is not straight. For simplicity, in our analysis the channel radius of curvature is assumed to be constant and the nondimensional ratio of curvature is defined as the ratio between the radius of curvature of the main channel centerline, R, and the width of the main channel, W. A series of simulations with different values of the riprap diameter, D50, was conducted to investigate how decreasing the radius of curvature, R, and/or increasing the floodplain width, Bf, affect the maximum value of the bed shear stress. No such laboratory investigations were conducted for curved channels. The numerical code was already validated using straight channel data. The fully 3-D non-hydrostatic RANS solver is fully capable of resolving flow in curved channels containing large-scale obstructions (e.g., abutments).

3.1 Description of Test Cases and RANS Solutions

Simulations in channels containing wing-wall abutments at their sides were performed with different values of the riprap mean diameter, D_{50}, and for two different flow depths corresponding to normal flow conditions (flow depth in the main channel, y_m=0.1 m) and flood conditions (flow over the floodplain). More details are given in Wu et al. (2019) based on which the discussion below is based. The width of the main channel was kept constant, W=2 m. The difference between the bed elevation over the floodplain and over the main channel was 0.1 m.

This is also the length scale (H_{ref}=0.1 m) used to nondimensionalize the different variables. The velocity scale was V=0.4 m/s. The Reynolds number defined with the velocity and length scale was Re=40,000. For flood conditions, the relationship between the flow depth over the floodplain, y_f, and the main channel depth is $y_f=y_m$-0.1 m. Series of simulations were conducted for three values of the floodplain width: B_f=0 m, 0.4 m and 1.4 m (B_f/H_{ref}=0, 4 and 14). These series are denoted as Case I, Case II, and Case III respectively in table 3.1. For each case, simulations were conducted in straight channels (R/W=∞) and in curved channels with R/W=20, 10 and 2. Figure 3.1 shows the computational domain in the straight channel simulations corresponding to Case I, Case II, and Case III. Figure 3.2 shows the computational domains used in the Case II simulations with varying radii of curvature. The range of nondimensional channel curvatures, 2<R/W<20, is basically the same as the range used in HEC-15 (2005) to characterize the amplification of the bed shear stress at the outer bank of bendways. The amplification factor is needed as an input in riprap design formulas used for stream bank embankment protection. Outside of the riprap apron, the channel bed was covered with sand. Up to four different values of the riprap diameter (D_{50}=20 mm, 28 mm, 40 mm and 60 mm or D_{50}/H_{ref}=0.2, 0.28, 0.4 and 0.6) were used in the different series of simulations. The mean diameter of the sand was kept constant (d_{50}=0.82 mm). The riprap apron around each abutment was of rectangular shape (fig. 3.3).

For each test case, the inlet discharge was varied in a series of simulations until two of the simulations predicted a maximum bed shear stress over the riprap apron slightly larger and, respectively, slightly smaller than the critical value for riprap shear failure determined following the procedure outlined in Melville et al. (2007).

The nondimensional values of the critical bed friction velocity for riprap shear failure are $u_{\tau c}/V$=0.12, 0.145, 0.175 and 0.21 for D_{50}/H_{ref}=0.2, 0.28, 0.4 and 0.61, respectively. The mean streamwise velocity in the cross section containing the two abutments was used to calculate the Froude number, Fr. The length scale in the definition of Fr was $y=y_m$. This is because for wing wall abutments, the length of the abutment is basically equal to the length of the floodplain, so the region protected by the riprap stone extends into the main channel. The reported value of the Fr number is the interpolated value between the ones in the two simulations that predicted a slightly larger and, respectively, a lightly smaller value of $u_{\tau c}/V$.

Table 3.1 Matrix of test cases considered for the wing-wall abutment. Reproduced from Wu et al. (2019).

Case	B_f/H_{ref}	B_f/W	y_m/H_{ref}	R/H_{ref}	R/W	D_{50}/H_{ref}
Case I	0.0	0.0	1.0	∞	∞	0.20, 0.40
				400	20	0.20, 0.40
				200	10	0.20, 0.40
				40	2	0.20, 0.40
			1.7	∞	∞	0.20, 0.40
				200	10	0.20, 0.40
Case II	4.0	0.2	1.7	∞	∞	0.20, 0.28, 0.40, 0.61
				400	20	0.20, 0.28, 0.40, 0.61
				200	10	0.20, 0.28, 0.40, 0.61
				40	2	0.20, 0.28, 0.40, 0.61
Case III	14.0	0.7	1.7	∞	∞	0.20, 0.40, 0.61
				400	20	0.20, 0.40, 0.61
				200	10	0.20, 0.40, 0.61
				40	2	0.20, 0.40, 0.61

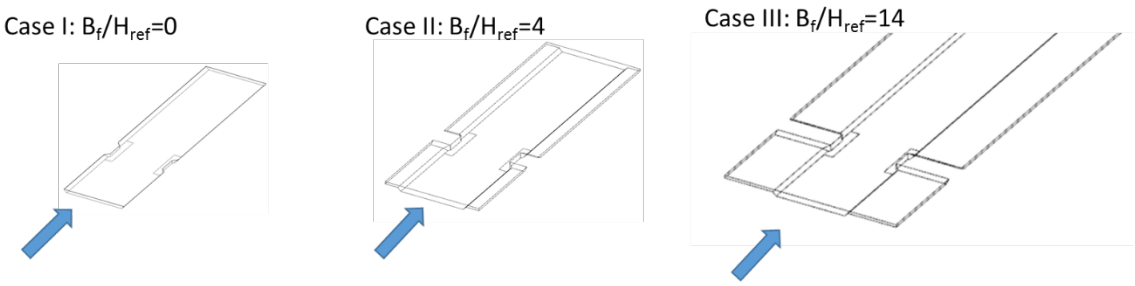

Figure 3.1 Sketch showing computational domain in the straight channel cases with different values of the nondimensional floodplain width, B_f/H_{ref}. Reproduced from Wu et al. (2019).

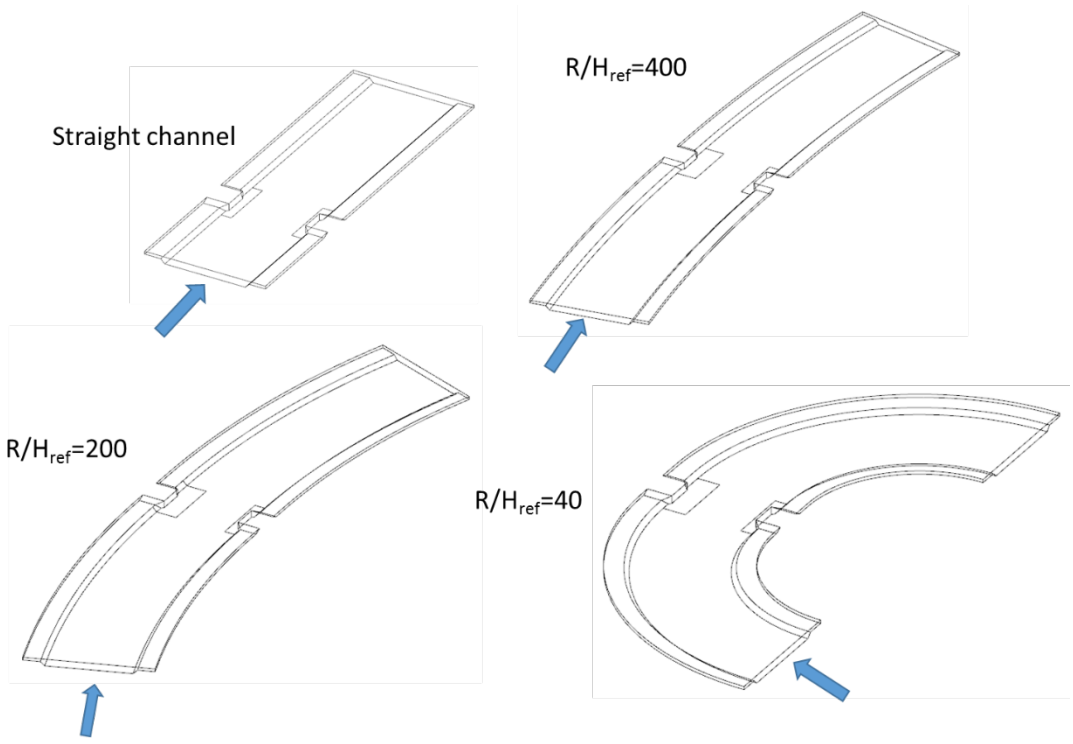

Figure 3.2 Sketch showing computational domain in the Case II simulations with different values of the nondimensional radius of curvature of the channel, R/H_{ref}.

Figure 3.3 shows a sketch of the general layout of the computational domain in one of the curved channel test cases (B_f/W=0), the transition region from the floodplain to the main channel and a cross section through the wing-wall abutment. The wing-wall abutment geometrical set up corresponds to that used in the laboratory experiments of Melville et al. (2007).

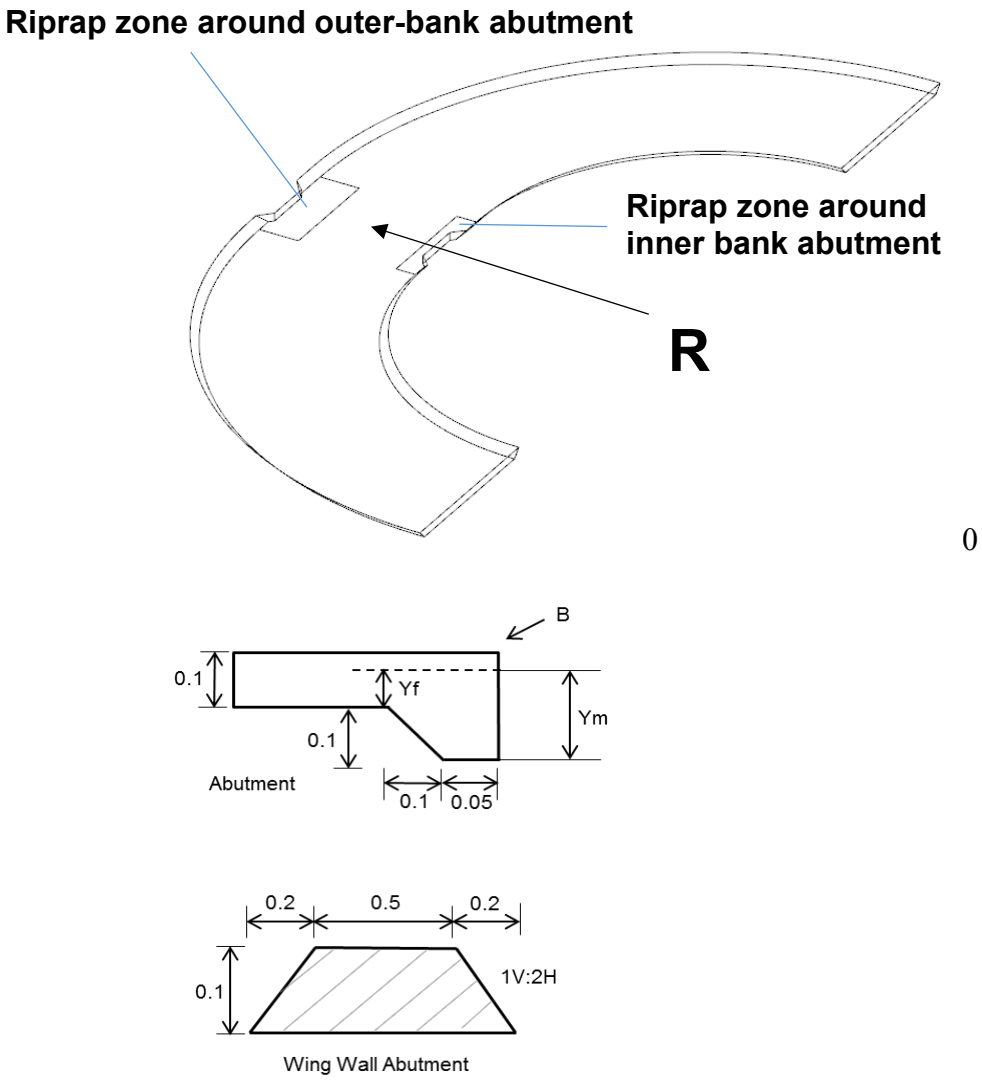

Figure 3.3 Sketch showing general layout in the simulations performed in a curved channel containing an abutment at each bank. Also shown are a cross section of the wing-wall abutment and the transition region between the main channel (water depth is y_m) and the floodplain (water depth is y_f). Dimensions are given in meters.

The main dimensions of the computational domain and the relative positions of the regions where the riprap stone protection was placed are shown in figures 3.4 and 3.5 for the straight channel simulations conducted for Case I and Case III, respectively. The dimensions of the riprap collar were kept constant for the inner-bank abutment. The width of the riprap collar

was $2.5H_{ref}$ for the inner bank abutments and $5H_{ref}$ for the outer-bank abutment. This increase was needed because the streamwise velocity around the outer-bank abutment is higher because of curvature induced effects, so a larger width of the riprap collar should be considered. Preliminary simulations showed that the predicted critical value of the Froude number was about the same if the width of the riprap apron was increased to $5H_{ref}$ for the two abutments in the straight channel simulations.

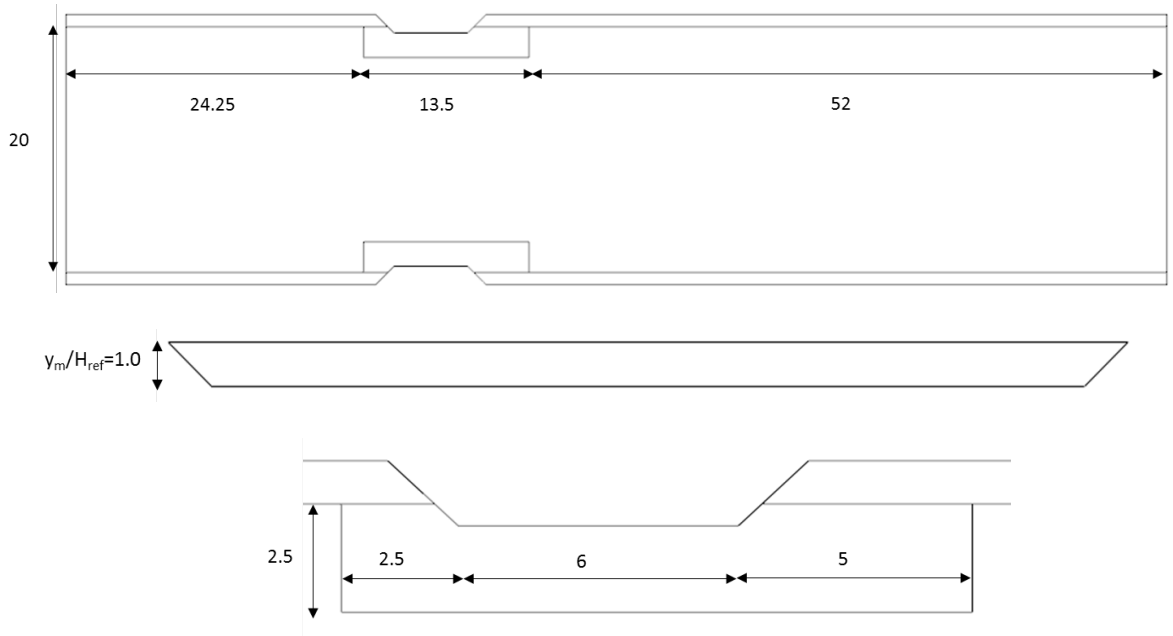

Figure 3.4 Computational domain used in the straight channel (Case I) simulations with B_f/H_{ref}=0. The view is from above. The middle frame shows a cross section of the channel that does not cut through the abutment. The lowest frame shows the spatial extent of the riprap apron in the straight channel simulations. All lengths were nondimensionalized with H_{ref}.

In the straight channel simulations, the distance between the inlet section and the abutment was kept constant ($24.25H_{ref}$), but the distance between the abutment and the outlet section was increased with increasing B_f/W due to the increase in the length of the recirculation regions generated over the floodplain, downstream of the abutments (see figures 3.4 and 3.5). In

the curved channel simulations, the streamwise length of the computational domain between the abutments and the inlet/outlet sections was varied with respect to the straight channel simulations to insure the regions where the flow patterns were affected by the presence of the two abutments did not reach the inlet and outlet boundaries.

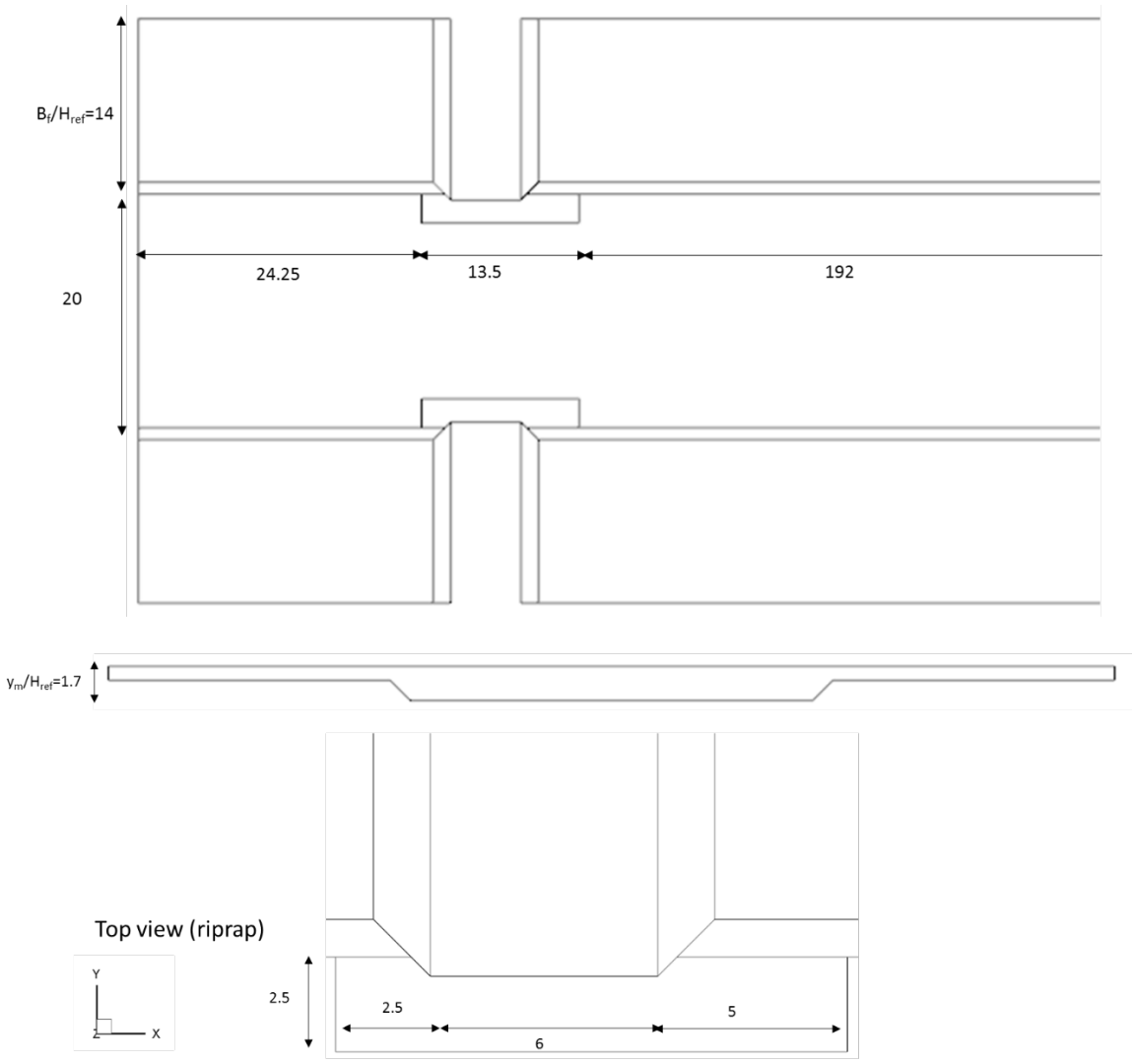

Figure 3.5 Computational domain used in the straight channel, Case 3 simulations with B_f/H_{ref}=14 (free surface elevation was situated above the floodplain level). The view is from above. The middle frame shows a cross section of the channel not cutting through the abutment. The lowest frame shows the spatial extent of the riprap apron in the straight channel simulations. All lengths were nondimensionalized with H_{ref}.

Figure 3.6 shows a view of the computational mesh near one of the abutments. For most simulations, the total number of computational cells was close to five million. The mesh was refined close to all solid boundaries, including the surfaces of the two abutments, to insure all the boundary layers were sufficiently well resolved. This is essential to accurately predict the mean flow and bed friction velocity distributions. The mesh around the abutments was unstructured. It was connected to a structured mesh upstream and downstream of the abutments and also in the main channel, away from the toe of each abutment. The level of mesh refinement near the abutments was the same in the straight and curved channel simulations. Grid dependencies studies were conducted to confirm the solutions and bed friction velocity distributions were grid independent.

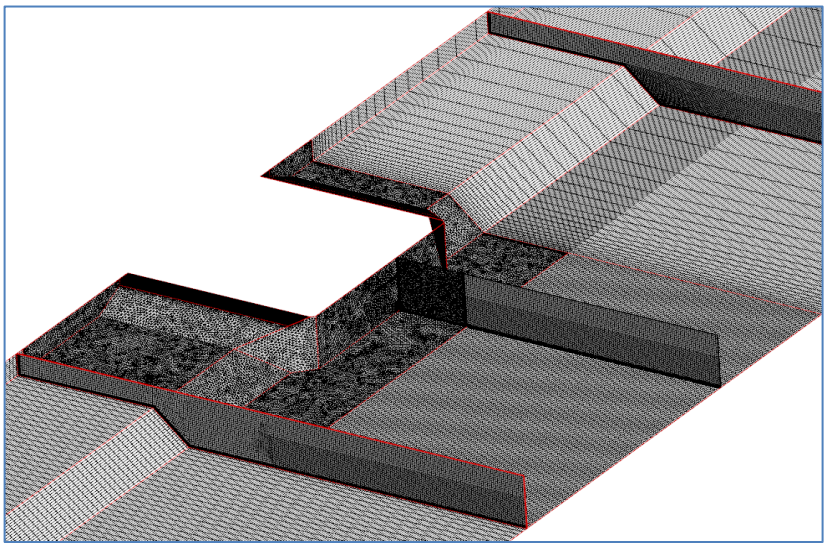

Figure 3.6 Grid used to mesh the computational domain in the Case II straight channel simulations. Only half of the domain is shown.

Figure 3.7 shows the effect of increasing the channel curvature, or equivalently of decreasing the radius of curvature, R, on the mean streamwise velocity distribution and 2-D

streamline patterns at the free surface for B_f/H_{ref}=4 (Case II, D_{50}/H_{ref}=0.61 simulations). For the straight channel case, the flow is symmetrical with respect to the channel centerline and the main recirculation regions downstream of the abutment have equal sizes.

a)

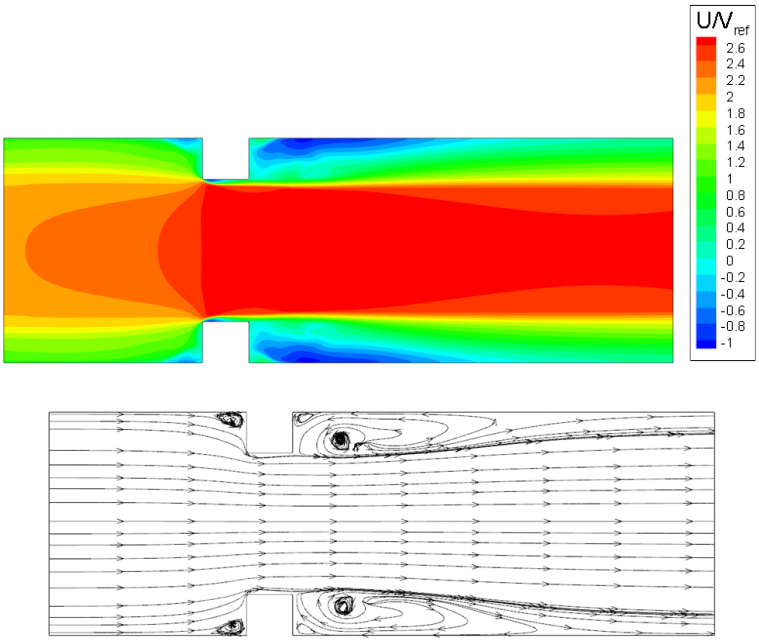

b)

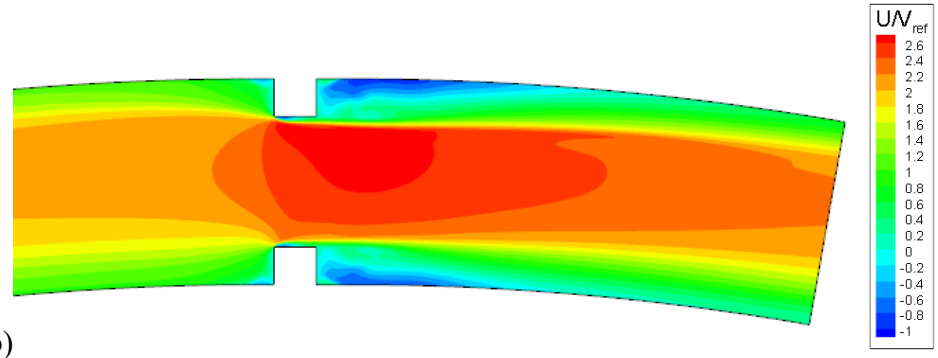

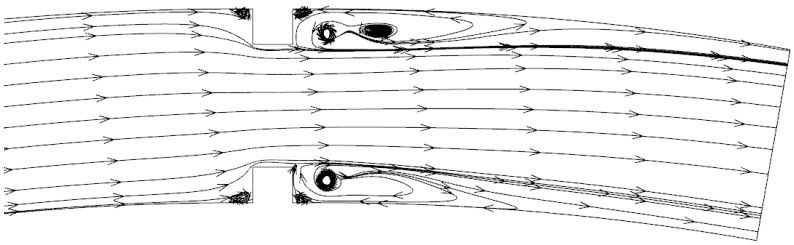

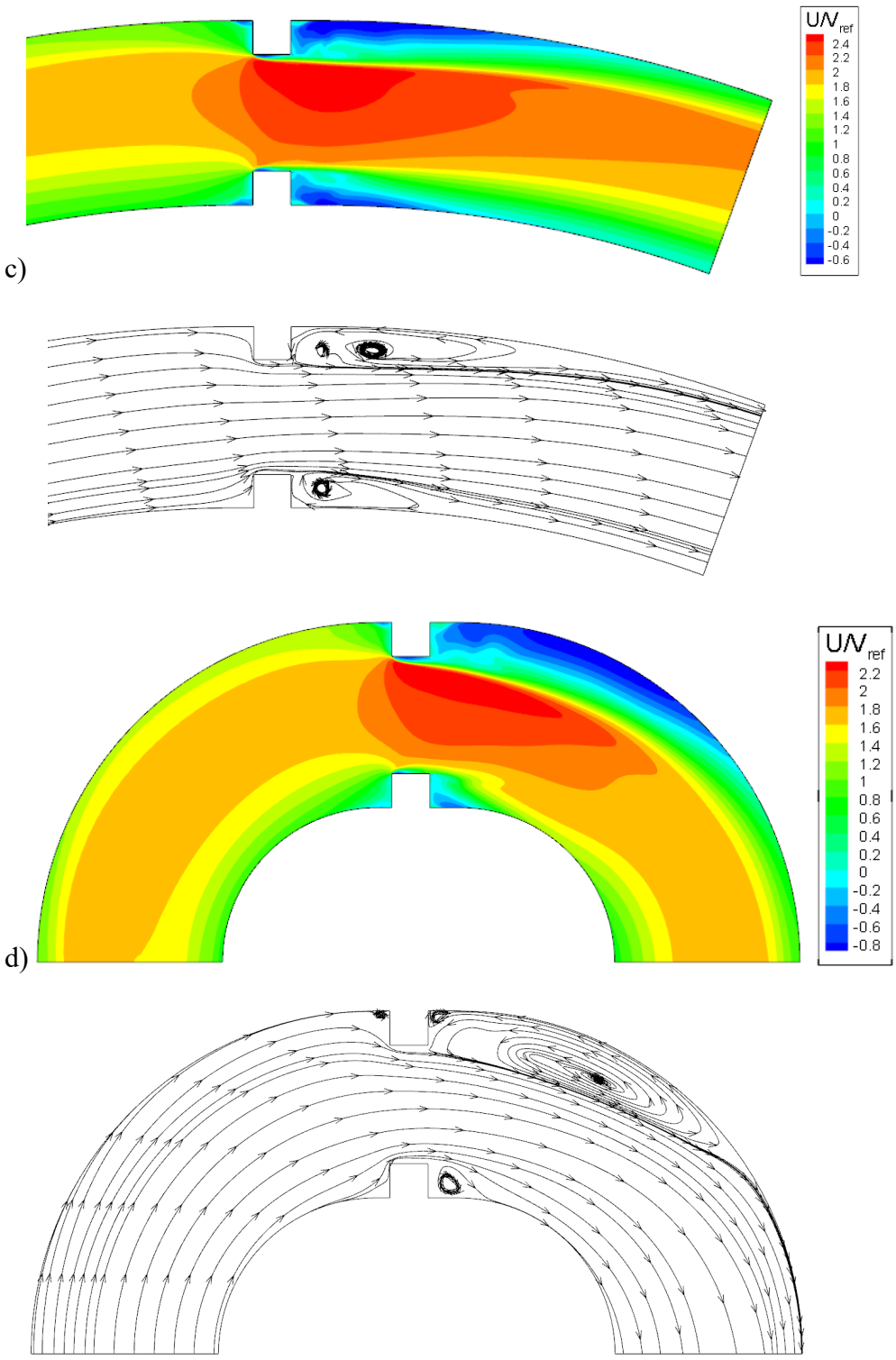

Figure 3.7 Visualization of the nondimensional streamwise velocity and 2-D streamline patterns at the free surface for Case 2 simulations with a riprap size D_{50}/H_{ref}=0.4. a) R/H_{ref}=∞; b) R/H_{ref}=400; c) R/H_{ref}=200; d) R/H_{ref}=40. Partially reproduced from Wu et al. (2019).

As the curvature increases, the region of high streamwise velocity moves closer to the outer bank abutment, while the streamwise velocity magnitude is reduced around the extremity of the inner-bank abutment. The length of the recirculation eddy downstream of the outer bank abutment increases with increasing channel curvature, while the opposite is true for the recirculation region forming downstream of the inner-bank abutment. This change in the position and size of the regions of high streamwise velocity near the free surface has a direct effect on the magnitude of the peak bed shear stress and the size of the regions of high bed shear stress around the two abutments.

To better visualize the effect of increasing the channel curvature on the bed shear stress magnitude, τ, figure 3.8 shows the distributions of τ/τ_{max} for two Case 1 simulations, where τ_{max} is the maximum bed shear stress over the riprap apron at the outer bank.

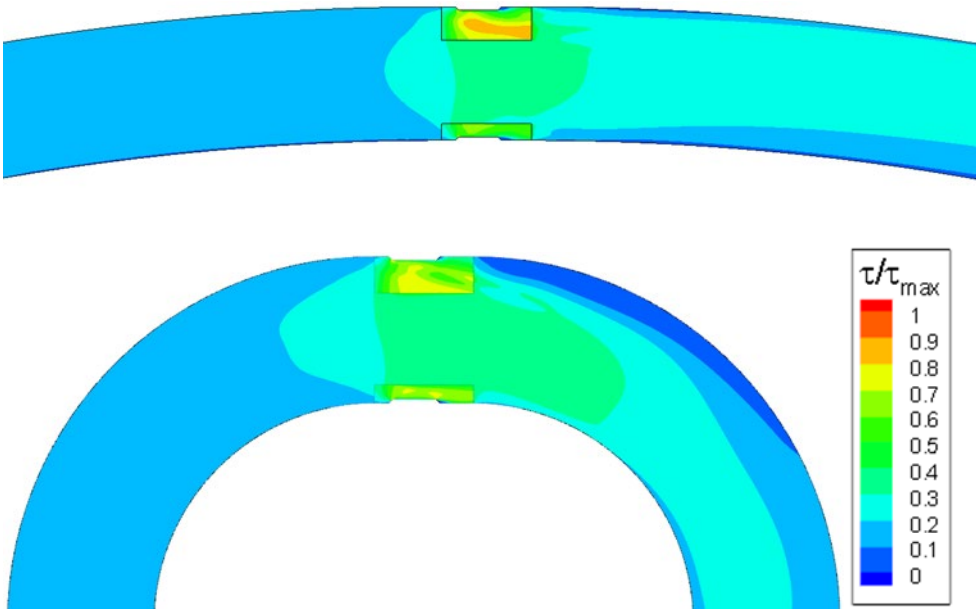

Figure 3.8 Effect of channel curvature on the nondimensional bed friction velocity distribution over the main channel and its floodplain for a riprap size D_{50}/H_{ref}=0.61 and no floodplain (B_f/H_{ref}=0). a) R/H_{ref}=400; b) R/H_{ref}=40.

The maximum bed shear stress was predicted close to the upstream edge of the outer-bank abutment (see fig. 3.9). A second, larger region of large bed shear stress formed downstream of the upstream corner of the outer-bank abutment's extremity. Also consistent with the free-surface streamwise velocity distributions, the predicted bed shear stresses were very low beneath the recirculation regions forming downstream of the two abutments (fig. 3.8). Outside of the two riprap aprons, the bed shear stresses were amplified beneath the region of large free-surface streamwise velocities (figures 3.7b, 3.7d and 3.8).

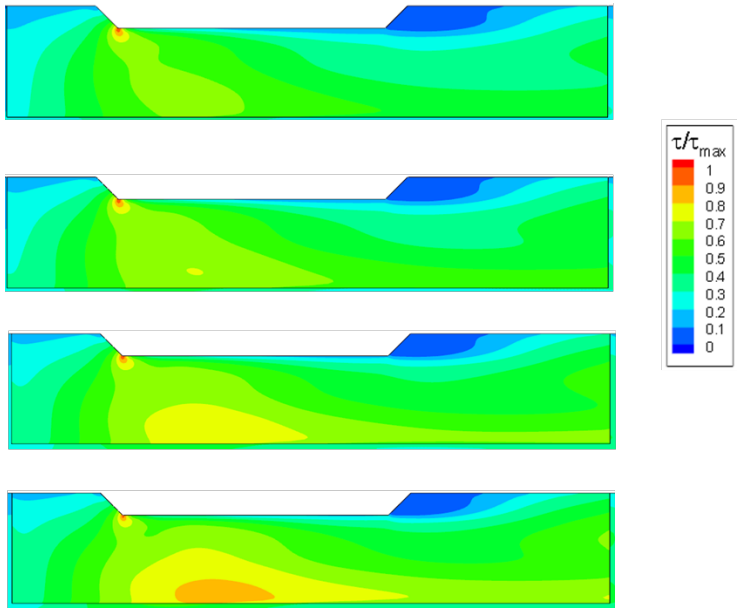

Figure 3.9 Effect of riprap size (D_{50}/H_{ref}=0.2, 0.28, 0.4, 0.61) on the nondimensional bed friction velocity distribution over the riprap layer at the outer-bank abutment for the straight channel ($R/H_{ref}=\infty$) Case II simulations.

Figures 3.9 to 3.12 show the distributions of τ/τ_{max} over the riprap apron at the outer bank abutment for Case II simulations. Each figure has four frames corresponding to simulation results obtained for different sizes of the riprap stone (D_{50}/H_{ref}=0.2, 0.28, 0.4, 0.61). In all these simulations τ_{max} is predicted very close to the upstream edge of the outer-bank abutment. This

simulation result is in agreement with the small-scale model observations of Pagan-Ortiz (1991) for local scour at vertical wing-wall abutments.

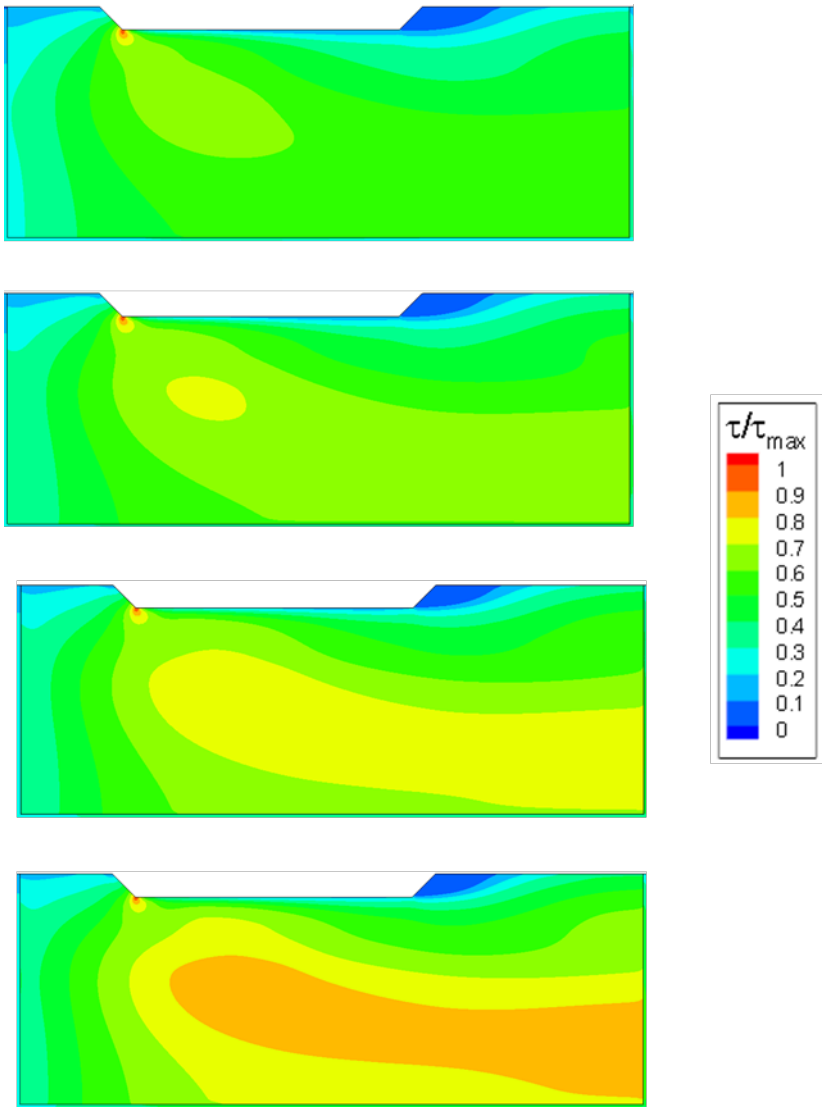

Figure 3.10 Effect of riprap size (D_{50}/H_{ref}=0.2, 0.28, 0.4, 0.61) on the nondimensional bed friction velocity distribution over the riprap layer at the outer-bank abutment for the curved channel (R/H_{ref}=400) Case II simulations. Partially reproduced from Wu et al. (2019).

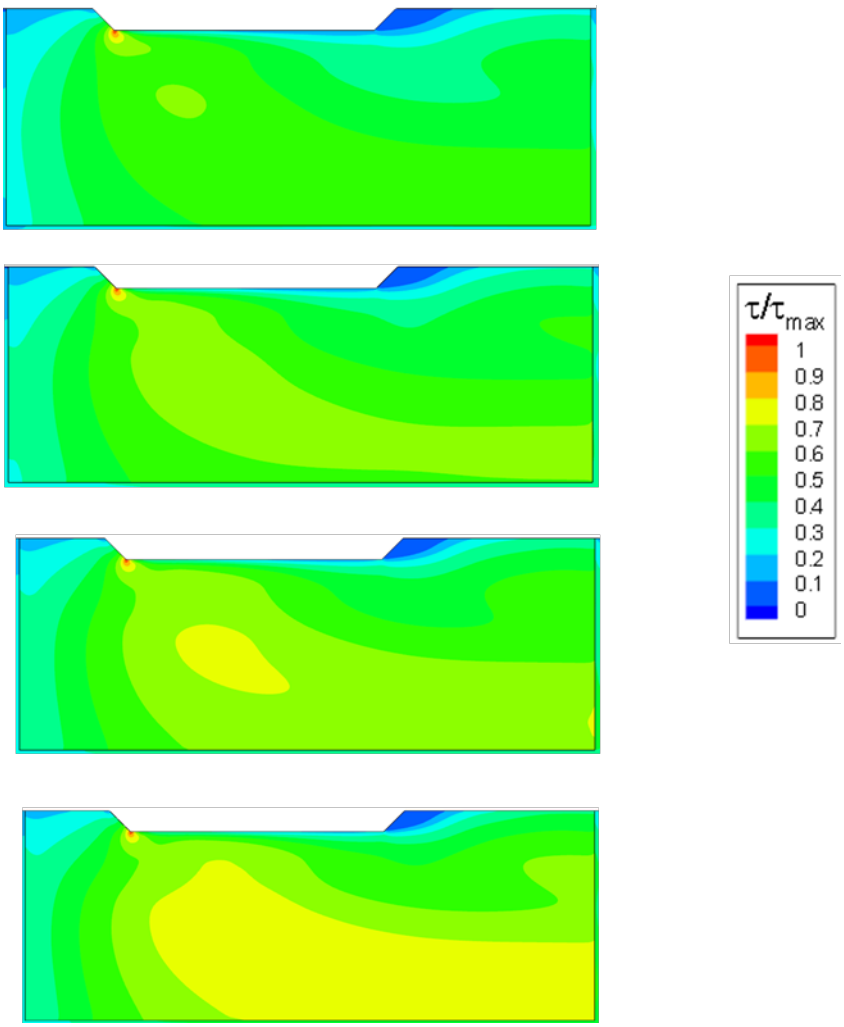

Figure 3.11 Effect of riprap size (D_{50}/H_{ref}=0.2, 0.28, 0.4, 0.61) on the nondimensional bed friction velocity distribution over the riprap layer at the outer-bank abutment for the curved channel (R/H_{ref}=200) Case II simulations. Partially reproduced from Wu et al. (2019).

In the straight channel simulations (fig. 3.9), the main effect of increasing the riprap stone diameter is to increase the size and peak values inside the second region of relatively large bed shear stress values (e.g., peak τ/τ_{max} values are around 0.7 for D_{50}/H_{ref}=0.28 and around 0.9 for D_{50}/H_{ref}=0.61) situated close to the outer edge of the riprap apron. It is possible that for an even larger riprap stone diameter, the peak bed shear stresses will occur next to the outer side extremity of the riprap apron rather than close to the upstream edge of the outer-bank abutment.

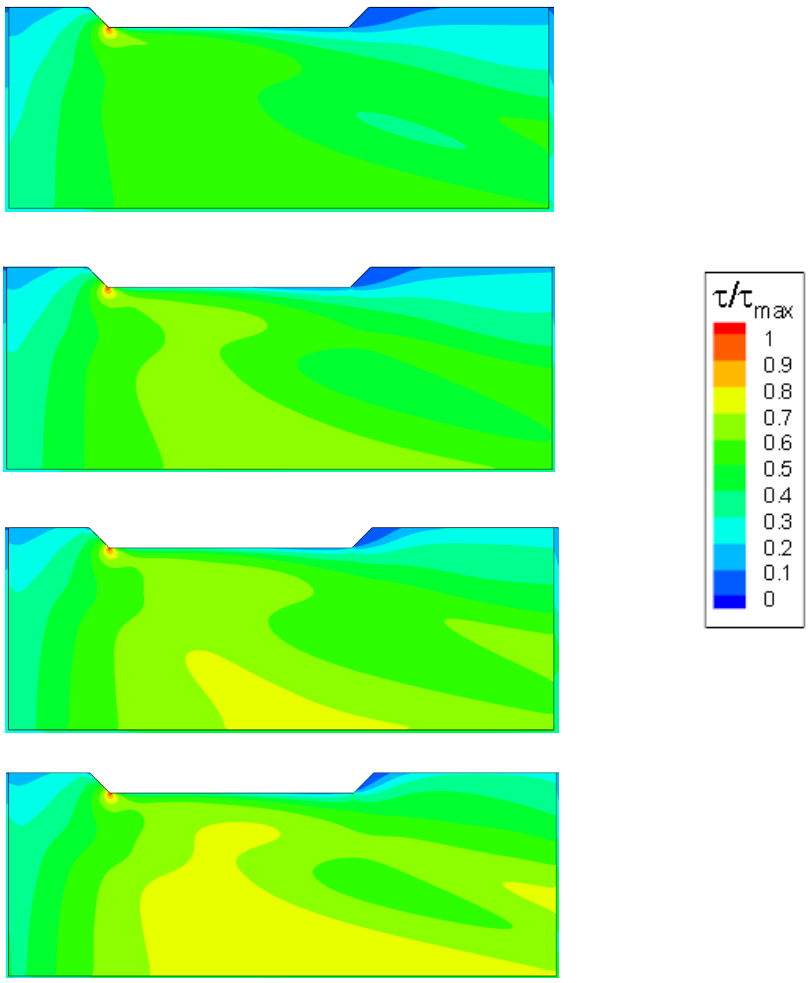

Figure 3.12 Effect of riprap size (D_{50}/H_{ref}=0.2, 0.28, 0.4, 0.61) on the nondimensional bed friction velocity distribution over the riprap layer at the outer-bank abutment for the curved channel (R/H_{ref}=40) Case II simulations. Partially reproduced from Wu et al. (2019).

These trends are also observed in the R/H_{ref}=400 curved channel simulations shown in Figure 3.10, where the rate of growth of the size of the second region of high τ/τ_{max} with increasing D_{50} is larger than that observed in the straight channel simulations. The second region of large bed shear stress forms over the middle part of the riprap apron and extends until the downstream end of the riprap apron. This is the curvature for which the largest increase of τ/τ_{max} with increasing D_{50} is observed inside the second region of high τ/τ_{max}. As the curvature is further increased (figures 3.11 and 3.12), the peak τ/τ_{max} values inside this second region of high

bed shear stress still increase with increasing D_{50} but the rate of increase is smaller than that observed in the R/H_{ref}=400 simulations. So, one can conclude that both channel radius of curvature and riprap stone diameter have a clear effect on the bed shear stress distributions over the riprap apron. Similar conclusions were reached for Case I and Case III simulations. For brevity, the bed friction velocity distributions are not included for the Case I and Case III simulations. Of course, for riprap sizing what matters is how R and D_{50} affect the peak bed shear stress value. These effects are discussed in the next subsection based on the results obtained by Wu et al. (2019).

3.2 Effect of Channel Radius of Curvature and Riprap Diameter on the Critical Froude number.

Figure 3.13 summarizes the variation of the critical Froude number with D_{50}/y_m, where the Froude number is calculated with the flow depth in the main channel, y_m and the mean velocity in the cross section cutting through the symmetry plane of the two abutments. Also represented in the same figure are the critical Froude number predictions given by the design formulas of Lagasse et al. (2001) and Pagan-Ortiz (1991) proposed for wing-wall abutments placed in straight channels. One can see that for a fixed riprap stone diameter, fixed flow depth and floodplain width, the critical Froude number decreases as the channel curvature increases. This means that riprap stone will start being entrained by the flow at smaller mean channel velocities/discharges with decreasing R/W. As more clearly seen from figure 3.14, where the data for Cases I, II and III were plotted separately, the effect of increasing the bank curvature on the decay of the critical Froude number is the largest for channels with no floodplain and decreases monotonically with increasing floodplain width. For example, in Case I, Fr decreases from 0.75 for $R/H_{ref}=\infty$ to 0.55 for R/H_{ref}=40 if $D_{50}/y_m\approx$0.38 (fig. 3.14a). Meanwhile, in Case III, Fr decreases only from 0.55 for $R/H_{ref}=\infty$ to 0.5 for R/H_{ref}=40 if $D_{50}/y_m\approx$0.38 (fig. 3.14c). The

decay of Fr with increasing bank curvature is expected given that the free-surface streamwise velocity distributions showed an increase of the maximum values around the outer-bank abutment with increasing channel curvature. For the cases with $B_f>0$ (Case II and Case III), the critical Froude number decreases with increasing floodplain width assuming D_{50}, y_m and R are kept constant.

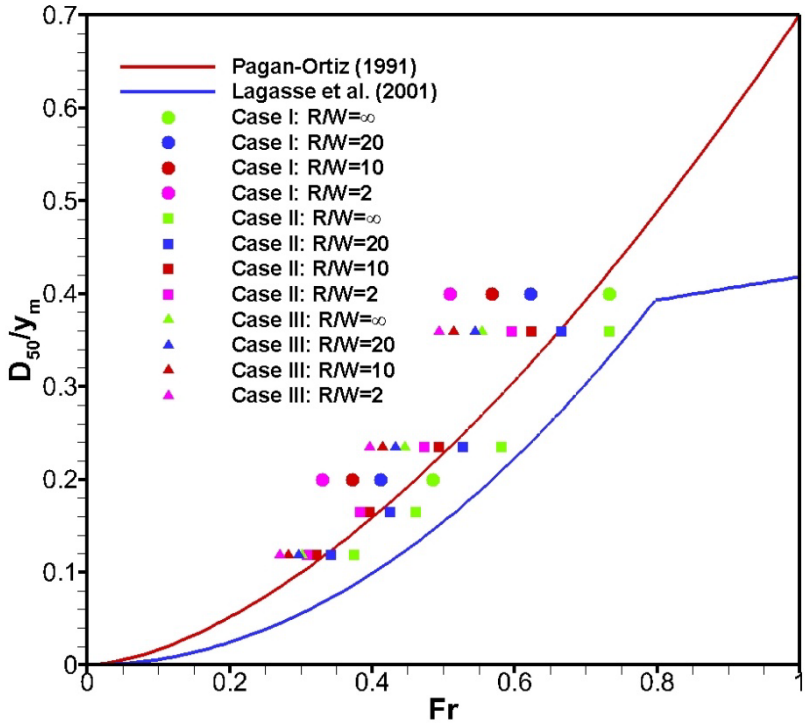

Figure 3.13 Comparison of numerical results for wing-wall abutments in straight and curved channels for Cases I, II and III with Lagasse et al. (2001) and Pagan-Ortiz (1991) equations. Reproduced from Wu et al. (2019).

Another interesting observation is that the critical Froude numbers predicted in the straight channel simulations of Cases I and II fell in between the values given by Pagan-Ortiz (1991) and Lagasse et al. (2001) formulas. However, even Pagan-Ortiz (1991) formula overestimates the critical Froude number for Case III simulations, meaning the formula is not

conservative enough for channels with a very wide floodplain. This is not so surprising because both formulas were proposed based on experiments conducted with no floodplain or relatively narrow floodplains (e.g., similar to Case II).

Before trying to propose a formula that would fit all the data obtained from the numerical experiments, it is relevant to mention that both design formulas can be casted in a form that better illustrates their similarities. After some manipulations, Pagan-Ortiz formula can be written as:

$$D_{50}/y=(1.064/(S_s-1))^{0.81} *Fr^{1.62} \quad (3.1)$$

Lagasse et al. (2001) formula for Fr<0.8 can be written as:

$$D_{50}/y=(1.02/(S_s-1)) *Fr^{2} \quad (3.2)$$

where S_s is the specific gravity of riprap, typically equal to 2.65. This leads to the generic formula:

$$D_{50}/y=(K_s/(S_s-1))^{0.5\alpha}*Fr^{\alpha}=C^{\alpha/2}*Fr^{\alpha} \quad (3.3)$$

where K_s is the shape factor and $y=y_m$ for wing-wall abutments. Equivalently, one can define a model coefficient C that is directly related to the shape factor, $C=K_s/(S_s-1)$. So, C=0.645 and α=1.62 for Pagan-Ortiz (1991) formula and C=0.618 and α=2.0 for Lagasse et al. (2001) formula (Fr<0.8). All design formulas give Fr only as a function of D_{50}/y. This means that the effect of

the relative floodplain width, B_f/W, is ignored or considered to be negligible. No formula tried to account for the effect of channel curvature.

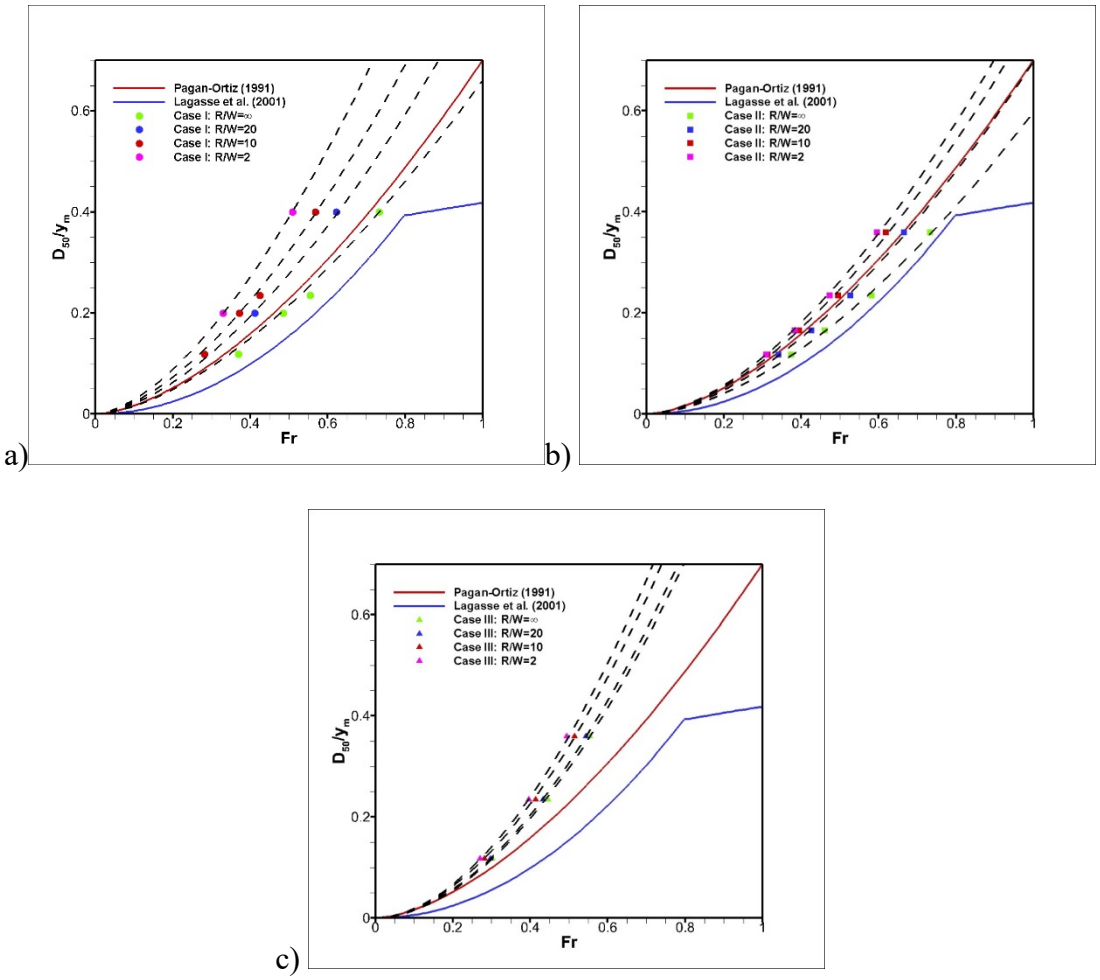

Figure 3.14 Comparison between the numerical predictions of the critical Froude number and Lagasse et al. (2001) and Pagan-Ortiz (1991) equations for wing-wall abutments in straight and curved channels. a) Case I; b) Case II; c) Case III. The dashed lines represent the modified formula (3.3) using the α and C values from Table 3.2. Reproduced from Wu et al. (2019).

The fact that Fr increases faster with increasing D_{50}/y_m as the channel curvature increases suggests either a larger value of α or a larger vaue of C should be used in formula (3.3) to fit the data.

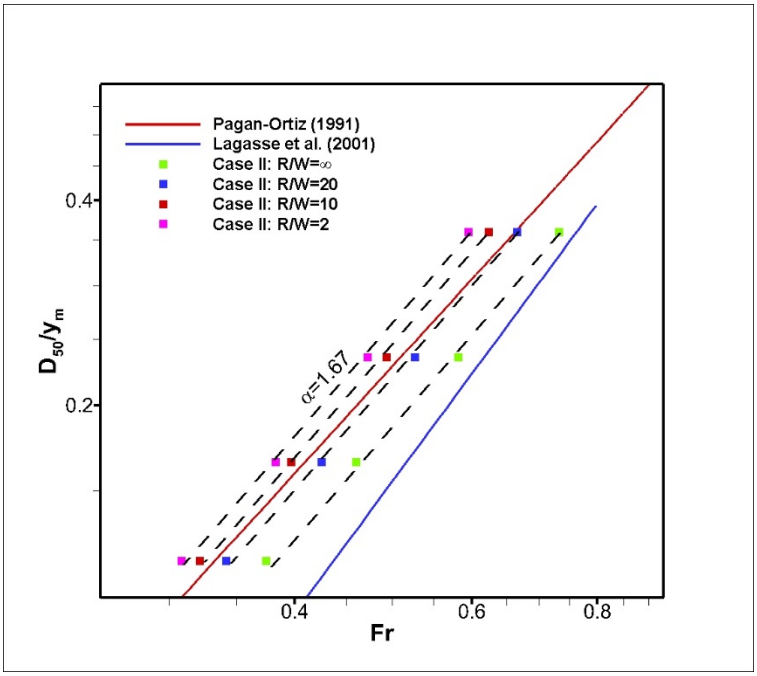

Figure 3.15 Critical Froude number as a function of D_{50}/y_m for Case II simulations. A straight line with a slope α=1.67 fits fairly well the different simulations performed with 4 different values of D_{50}. Also shown are the straight lines corresponding to Lagasse et al. (2001) and Pagan-Ortiz (1991) equations for which α=1.62 and α=2, respectively. Reproduced from Wu et al. (2019).

The variation of Fr with increasing D_{50}/y_m for different values of B_f/H_{ref} or B_f/W can be easily inferred by plotting Fr vs. D_{50}/y_m in log-log scale. Figure 3.15 shows the results for Case II simulations with B_f/H_{ref}=4. The main two findings are that a power law accurately describes the variation of Fr with D_{50}/y_m for each value of the channel radius of curvature, R, and that the value of α is close to independent of R. While the former finding is somewhat expected, the fact that, for a fixed floodplain width, the same value of the power exponent can be used to describe the variation of Fr with D_{50}/y_m for different R values should help obtain a simple general formula for wing-wall abutments placed in curved channels. For Case II (B_f/H_{ref}=4) simulations, figure 3.15 shows that the best fit value is α=1.67. Analysis of Cases I and III confirmed that α is independent of R, but the best fit value was different (α=1.62 for Case I and α=1.84 for Case 2).

This means that α is a function of the floodplain width, B_f. The value inferred based on Case I simulations with no floodplain is exactly the same as the value (α=1.62) used in Pagan-Ortiz (1991) formula. Simulation data also show that α is monotonically increasing with B_f. For B_f/H_{ref}=14 the predicted value is α=1.84. This value is closer, but still smaller, than the value (α=2) used in Lagasse et al. (2001) formula for Fr<0.8.

Table 3.2 Best fit values of the power coefficient α and of the coefficient C as a function of the radius of curvature R and floodplain width, B_f. Reproduced from Wu et al. (2019).

	$R/H_{ref}=\infty$ R/W=∞	$R/H_{ref}=400$ R/W=20	$R/H_{ref}=200$ R/W=10	$R/H_{ref}=40$ R/W=2
$B_f/H_{ref}=0.0$ $B_f/W=0$	α=1.62 C=0.60	α=1.62 C=0.82	α=1.62 C=0.99	α=1.62 C=1.25
$B_f/H_{ref}=4.0$ $B_f/W=0.2$	α=1.67 C=0.54	α=1.67 C=0.65	α=1.67 C=0.75	α=1.67 C=0.81
$B_f/H_{ref}=14.0$ $B_f/W=0.7$	α=1.84 C=1.07	α=1.84 C=1.11	α=1.84 C=1.24	α=1.84 C=1.32

Table 3.2 summarizes the values of α and of the model coefficient C for the simulations performed with varying floodplain width and radius of curvature. For straight channels with no floodplain and with a narrow floodplain, the inferred values of the model constant are C=0.54 and C=0.6. These values are fairly close to the value (C=0.646) in Pagan-Ortiz (1991) formula and the one (C=0.618) in Lagasse et al. (2001) formula assuming S=2.65. However, our data shows that these formulas are not conservative enough even for straight channels if the floodplain width is very large (e.g., for B_f/W>0.3).

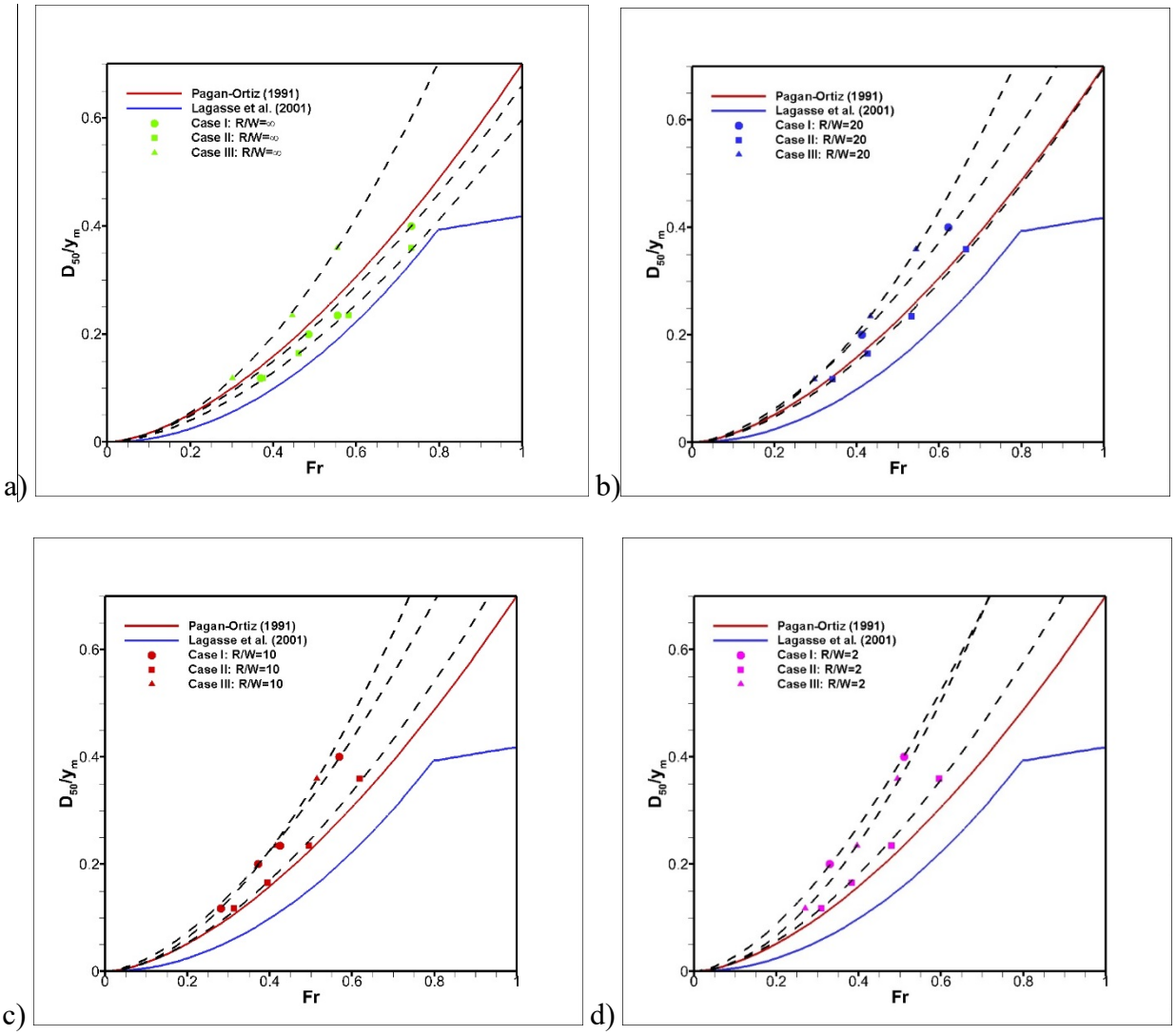

Figure 3.16 Critical Froude number as a function of floodplain width and D_{50}/y_m. a) straight channel, $R/H_{ref}=\infty$; b) $R/H_{ref}=400$, $R/W=20$; c) $R/H_{ref}=400$, $R/W=10$; d) $R/H_{ref}=40$, $R/W=2$. The dashed lines represent the modified formula (3.3) using the α and C values from Table 3.2. Frame a is reproduced from Wu et al. (2019).

Results in table 3.2 also show that C is not varying monotonically with increasing floodplain width. The C values for $B_f/H_{ref}=0$ are 10-30% larger than the values for $B_f/H_{ref}=4$. The largest C values are observed for $B_f/H_{ref}=1.4$. This effect is attributed to the fact that the flow patterns in the simulations with no floodplain are quite different from those in the simulations where a floodplain is present. Most probably C is monotonically increasing with increasing B_f

past a threshold value of the floodplain width. Results in table 3.2 also show that the effect of increasing the curvature, W/R, is to increase C. Meanwhile, C is monotonically decreasing with increasing B_f. For example, C_{max}/C_{min}=2.1 for Case I (B_f/W=0), C_{max}/C_{min}=1.5 for Case II (B_f/H_{ref}=4, B_f/W=0.2) and C_{max}/C_{min}=1.2 for Case III (B_f/H_{ref}=14, B_f/W=0.7). This suggests that C will become close to constant (e.g., independent of channel curvature) for very large B_f/W.

Figure 3.16 replots the data in figure. 3.13 together with the curves corresponding to the modified design formula, in which the values of α and C are given in table 3.2. A good agreement between the design formula predictions and the values inferred from the numerical experiments is observed for all test cases.

Chapter 4 Conclusions, Recommendations, and Proposed Future Work

Reliable and safe transportation infrastructure design for flooding events is of great economic importance for state and federal agencies in charge of maintaining our road operations. Bridges are major structures that need to be protected against severe local scour around their abutments. Existing guidelines to place riprap stone do not always provide effective protection against erosion at bridge abutments. The main reason is that these guidelines were developed based on a limited set of laboratory experiments performed with a fairly narrow range of the main variables controlling riprap shear failure. All of these laboratory experiments were conducted in straight channels. In principle, these formulas should not be used for cases where the abutments are placed in a region where channel curvature effects may be significant.

As part of the present research project, a general methodology based on 3-D non-hydrostatic RANS numerical simulations was developed to determine the conditions for riprap shear failure for cases when a riprap apron is placed close to each abutment. The relationship proposed by Melville and Coleman (2000) and Melville et al. (2007) for riprap entrainment threshold (shear failure mode) was used to determine if riprap stone entrainment occurs. The methodology was validated during Year 1 for wing-wall abutments using the experimental data of Melville et al. (2007). The proposed numerical approach is much less expensive compared to the classical one based on laboratory investigations conducted in a flume and allows incorporating additional complexities present at many bridge sites in the field.

In the second year, a large set of simulations was performed in straight and curved channels of constant width W containing two wing-wall abutments. Cases with no floodplain ($B_f/W=0$) and with a floodplain of increasing width ($B_f/W=0.2$ and 0.7) were considered. In the curved channel simulations, the nondimensional ratio of curvature, R/W, was varied between 2

and 20. This range covers most of the cases when abutments are placed in regions where channel curvature is not negligible. Simulations were performed with different values of the riprap stone mean diameter and for two different flow depths corresponding to normal flow (flow only inside the main channel) and flood conditions (flow over the floodplain and the main channel).

The numerical simulations allowed understanding how increasing channel curvature and/or increasing floodplain width affect the maximum bed shear stress over the riprap apron protecting the abutment and the critical Froude number for riprap shear failure. Based on data from the numerical experiments, the performance of existing design formulas (Pagan-Ortiz,1991 and Lagasse et al., 2001) used for riprap protection at bridges containing wing-wall abutments was checked for a wide range of conditions, outside of the range that was used to calibrate these design formulas. A main finding was that the two design formulas are not conservative enough if the floodplain width is relatively large, even for the case of a straight channel. The other finding was that the two design formulas are not conservative enough for channels of sufficiently large curvature. This result was somewhat expected given that the increased acceleration of the flow around the outer-bank abutment with increasing channel curvature should also result in an increase of the maximum bed shear stress over the riprap apron.

The other main contribution of the present research was to propose a new design formula that retains the same functional relationship as that of Pagan-Ortiz (1991) and Lagasse et al. (2001) formulas in which the non-dimensional riprap stone diameter, D_{50}/y_m, is proportional to the critical Froude number at a power α ($D_{50}/y_m=C^{\alpha/2}*Fr^{\alpha}$). Rather than using constant values for the two model parameters, C and α, as was the case for the previously mentioned formulas, in the new design formula C and α are a function of the main nondimensional geometrical parameters (e.g., B_f/W, R/W). One major finding is that α is not a function of the channel

curvature but increases monotonically with increasing B_f/W. The predicted range $1.62<\alpha<1.84$ was in between the values used by Pagan-Ortiz (1991) formula ($\alpha=1.62$) and Lagasse et al. (2001) formula ($\alpha=2$). The variation of C with increasing B_f/W is not monotonic because larger C values are predicted for channels with no floodplain compared to channels with a narrow floodplain. Meanwhile, C increases monotonically with decreasing R/W (e.g., with increasing curvature). The rate of increase is the largest for channels with no floodplain. Present data suggests that C is not a function of channel curvature for channels with very wide floodplains. The two-parameter formula can be used to predict the critical value of the Froude number, or equivalently the mean channel velocity or the discharge, at which riprap stone will start being entrained in straight and curved channels with or without a floodplain.

We will work with the Transportation Research Board committee TRB-AFB60 such that the main findings and the proposed new two-parameter design formula for determining minimum riprap size at wing-wall abutments will be considered for adoption in future releases of HEC 23. The proposed procedure described in the present report will be applied for spill-through abutments to obtain a modified design formula that can predict riprap shear failure taking into account the effects of channel curvature. The main challenge in generating the data sets is that one additional geometrical parameter has to be considered for spill-through abutments (e.g., the ratio between the abutment length and the floodplain width). This will increase substantially the number of simulations needed to develop a design formula compared to the present study that focused on wing-wall abutments. However, the basic procedure that will lead to an improved riprap design formula for spill-through abutments should be essentially the same.

Given the fact, that the present approach can be applied for any type of bridge abutments and piers, the present research has the potential to increase the efficiency of scour protection

measures at small bridges in the United States. Once adopted, the new procedure will enhance the capabilities of state DOTs to develop more reliable approaches to protect small bridges against possible failure induced by severe erosion associated with flood events. At a more general level, more accurate riprap design formulas for protection of abutments against erosion will result in significant reduction of the costs to operate roads during and after flood events. It will also contribute to reducing the risk for hazards associated with bridge failure during floods by avoiding structural failure.

References

Cardoso, A., Simarro, G. and Schleiss, A. 2010. "Sizing of riprap for spill-through abutments," *Water Management*, 163, issue WM10, 499-507, Paper 900024.

Cheng, Z., Koken, M. and Constantinescu, G. 2018. "Approximate methodology to account for effects of coherent structures on sediment entrainment in RANS simulations with a movable bed and applications to pier scour" *Advances in Water Resources,* 120, 65-82

Ettema, R, Constantinescu, G and Melville, B. 2011. "NCHRP 24-27(01): Evaluation of bridge pier scour research: scour processes and estimation" Final report for NCHRP.

HEC-23 Bridge scour and Stream Instability Countermeasures [Lagasse, P, Zevenberger,L., Schall, J and Chopper, P (2001), 'Bridge scour and stream instability countermeasures,' *Rep. No. FHWA-NH1-01-003*, Hydraulic Engineering Circular No. 23, 2nd Ed. Office of Bridge Technology, Federal Highway Administration, Washington DC]

HEC-23 Bridge scour and Stream Instability Countermeasures: Experience. Selection and Design Guidance, 2009, 3rd Edition

Horna Munoz, D. and Constantinescu, G. 2016. "A numerical study of the efficiency of flood protection structures," *International conference on fluvial hydraulics, River Flow 2016*, Saint Louis, USA.

Horna-Munoz, D. and Constantinescu, G. 2017. "Three dimensional numerical modeling of dam break flows," *4th International Symposium of Shallow Flows*, Eindhoven University of Technology, The Netherlands, June 2017

Horna-Munoz, D. and Constantinescu, G. .2018. "A fully 3-D numerical model to predict flood wave propagation and assess efficiency of flood protection measures" Advances in Water Resources*,* 122, 148-165

Hoffmans, G. J. C. M. and Verheij, H. J. 1997. “Scour manual.” A.A. Balkema, Rotterdam, Netherlands.

Melville, B. W. and Coleman, S. E. 2000. ”Bridge scour.” Water Resources Publications, Littleton, Colorado.

Melville, B., van Ballegooy, S., Coleman, S. and Barkdoll, B. 2006a. “Countermeasures to protection at spill-through abutments,” *J. Hydr. Engrg.*, 132:235-245.

Melville, B., van Ballegooy, S., Coleman, S. and Barkdoll, B. 2006b. “Scour countermeasures for wing wall abutments,” *J. Hydr. Engrg*., 132:563-574.

Melville, B., van Ballegooy, S., Coleman, S. and Barkdoll, B. 2007. “Riprap selection at wing wall abutments,” *J. Hydr. Engrg.,* 133:1265-1269.

NCHRP Project 24-18 (*NCHRP Report 587*), “Countermeasures to Protect Bridge Abutments from Scour”

NCHRP Project 24-19, “Selection Criteria and Design Guidelines, and techniques for the Size and Placement of Environmentally Sensitive Channel and Bank Protection Measures, and Quality Control”

NCHRP Project 24-20, “Prediction of Scour at Bridge Abutments”

Pagaz-Ortiz, J. 1991. “Stability of rock riprap for protection at the toe of abutments located at the flood plain,” *Rep. No. FHWA-Rd-91-057*, Federal Highway Administration, US Dept. of Transportation, Washington, DC.

Sumer, B. M. and Fredsoe J. 2002. “The mechanics of scour in the marine environment.” World Scientific.

Wu, H., Zen, J. and Constantinescu, G. (2019). A multiparameter design formula for riprap size selection at wing-wall abutments, Journal Hydraulic Research, paper TJHR-2019-0218